J Physiol 603.9 (2025) pp 2801–2819

The Journal of Physiology

Corticothalamic modulation of somatosensory thalamic tactile processing

Avisar Einav and Rony Azouz

Department of Physiology and Cell Biology, The School of Brain Sciences and Cognition, Ben-Gurion University of the Negev, Negev, Israel

Handling Editors: Katalin Toth & Kathy Ruddy

The peer review history is available in the Supporting Information section of this article (https://doi.org/10.1113/JP287526#support-information-section).

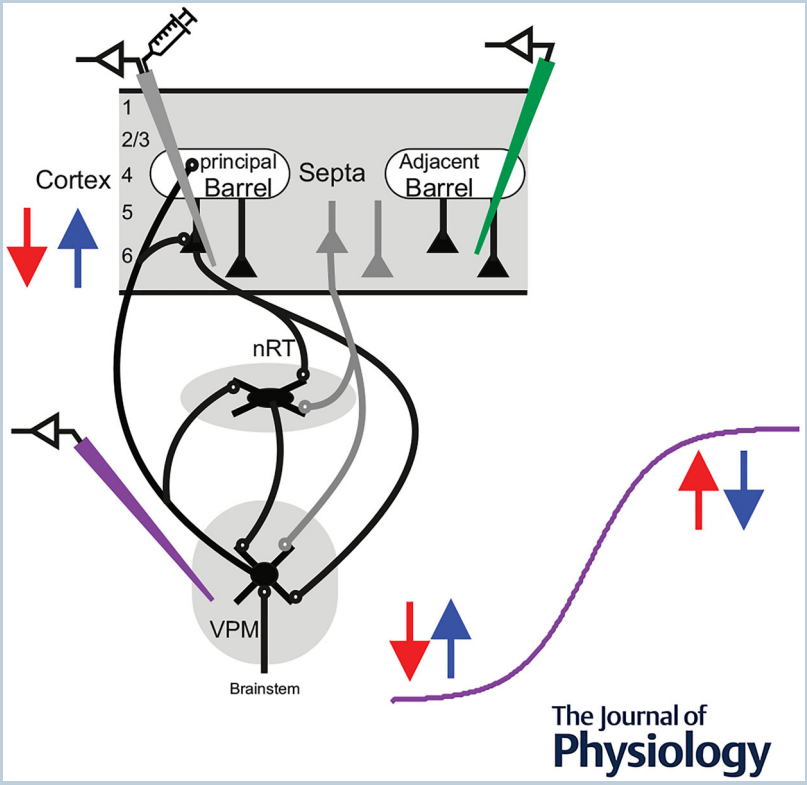

Abstract figure legend To examine how Layer 6 drug application affects ventral-posterior-medial (VPm) responses, we recorded local field potentials and single-unit activity from barrels adjacent to the drug application site during spontaneous and tactile stimulation. This approach allowed us to assess the influence of cortical feedback, given the reciprocal anatomical connections between VPm and cortex. Increasing cortical excitability (blue) amplified VPm responses to weaker stimuli but attenuated responses to stronger stimuli. Conversely, decreasing cortical excitability (red) reduced responses to weaker stimuli while enhancing responses to stronger stimuli.

Avisar Einav holds a bachelor's degree in neuroscience from Bar-Ilan University and later pursued a master's degree in medical sciences at Ben-Gurion University of the Negev under the supervision of Professor Rony Azouz. The research focused on somatosensory thalamic tactile processing. For the past 14 years Einav has been working as a software developer and currently leads a team developing flight simulators. **Rony Azouz** holds a PhD from the Hebrew University of Jerusalem. Later he pursued a post-doctoral study at Charles Gray's laboratory, studying visual neuroscience. Since 2001, he has been working as an investigator in the Department of Physiology and Cell Biology at the Medical School of Ben-Gurion University of the Negev in Beer-Sheva, where he studies the neuronal basis of sensory processing in the whisker somatosensory system of rodents.

DOI: 10.1113/JP287526

Abstract The brain's processing of sensory information involves intricate interactions between feedforward and feedback pathways, including corticothalamic feedback. Although feedback from cortical Layer 6 to the sensory thalamus is known to regulate sensory signalling, its precise function remains elusive. This study delves into the impact of Layer 6 feedback on sensory transmission in the ventral posteromedial nucleus using *in vivo* electrophysiology recordings in lightly anesthetized rats. By local administration of drugs to the barrel cortex during thalamic recordings, we investigate how corticothalamic neurons influence the transformation of tactile stimuli into neuronal discharge characteristics. Our findings reveal that increasing cortical dynamics enhances thalamic response magnitude at low stimulus intensities but decreases it at high intensities, whereas reducing cortical dynamics produces the opposite effect. Moreover, we observe bidirectional cortical influence on thalamic neurons extending to stimulus magnitude-dependent sensory adaptation and burst propensity modulation by Layer 6 dynamics. Specifically, increased cortical dynamics reduce thalamic sensory adaptation and increase burst propensity at low stimulus intensities, with no observed change at high intensities, whereas decreased cortical dynamics elicit opposite effects. We show that thalamic neurons can discriminate between stimuli, with cortical influence varying by stimulus intensity. Increased cortical dynamics enhances discrimination at low intensities, whereas reduced dynamics has the opposite effect. Our findings suggest that cortical control of ventral posteromedial nucleus tactile transformation is not a binary switch but a dynamic modulator, adjusting thalamic transformations in real time based on cortical dynamics. This mechanism finely tunes sensory processing to meet environmental and behavioural demands.

(Received 20 August 2024; accepted after revision 7 March 2025; first published online 4 April 2025)
Corresponding author R. Azouz: Department of Physiology and Cell Biology, Faculty of Health Sciences, The School of Brain Sciences and Cognition, Ben-Gurion University of the Negev, Beer-Sheva, Israel. Email: razouz@bgu.ac.il

Key points

- The study investigates touch processing in the brain by examining interactions between brain regions. Specifically, we study how cortical Layer 6 influences sensory signal processing in the thalamus.
- We manipulated Layer 6 activity with drugs and observed resulting changes in thalamic touch responses.
- Increased cortical activity enhanced weak touch signals but dampened strong ones in the thalamus; lower activity had the opposite effect.
- Increased cortical dynamics reduced thalamic sensory adaptation and increased burst propensity at low stimulus intensities, with no change at high intensities.
- The study shows that the brain's control over how it processes sensory information is not just an on/off switch but a dynamic system that adjusts in real time to different situations.

Introduction

Sensory signals undergo significant transformations in the thalamus before reaching the cortex, involving intricate processes of transduction, amplification and further contextualization in forebrain sensory areas. Tactile information from the whisker system involves parallel motor-sensory loops. It is conveyed to the neocortex through trigeminothalamic pathways, where the thalamus is the primary gateway to the cerebral cortex. The transfer of tactile signals is a dynamic process characterized by reciprocal communication between the cortex and thalamus, highlighting the strong influence of the cortex on thalamic activity and, therefore, on its tactile whisker input (Groh et al., 2008; Mease et al., 2014; Temereanca & Simons, 2004).

Corticothalamic (CT) neurons, specifically Layer 6 (L6) CTs, emerge as crucial modulators in this intricate process. L6 CT neurons feature a dual connectivity pattern. They exhibit dense local connectivity with excitatory and inhibitory neurons within the cortical columns (Bortone et al., 2014; Bourassa & Deschˆnes, 1995; Briggs et al., 2016; Llano & Sherman, 2008; Winer et al., 2001; Zhang & Deschênes, 1997). Activation of L6 CT neurons induces

a net suppression of spontaneous and sensory-evoked activity in the cortex via direct connections onto local fast-spiking (FS) inhibitory neurons (Bortone et al., 2014; Kim et al., 2014). On the contrary activating L6 CT neurons scales down sensory-evoked responses in most layers of the cortical column (Olsen et al., 2012). Moreover, these neurons exhibit a long-range feedback projection to the thalamus through both direct monosynaptic excitation and disynaptic inhibition via axon collaterals that target the inhibitory thalamic reticular nucleus (TRN), which, in turn, projects back to the thalamus. The intricate feedback connections, which account for approximately 30%–50% of the synapses in sensory first-order thalamic nuclei (Adams et al., 2002; Liu et al., 1995; Sherman & Koch, 1986; van Horn et al., 2000), result in a complex impact on thalamic activity, leading to a combination of modest facilitation and suppression in thalamic responses (Binzegger et al., 2007; Bourassa & Deschˆnes, 1995; Denman & Contreras, 2015; Lefort et al., 2009; Mease et al., 2014; Olsen et al., 2012; Temereanca & Simons, 2004; Thomson, 2010; Zhang & Deschênes, 1997). This interplay also fosters a diverse range of potential effects on thalamic excitability, as highlighted in studies by Crandall et al. (Crandall et al., 2015), McCormick & von Krosigk (McCormick & von Krosigk, 1992) and Wolfart et al. (Wolfart et al., 2005). Thus the connections between L6 CT neurons exert a powerful influence on thalamic excitability, which is likely crucial but still not fully understood in thalamocortical sensory signalling.

To investigate the extent of influence exerted by L6 CT neurons on both spontaneous and stimulus-evoked spiking activity across the sensory thalamocortical circuit, we recorded from two specific brain regions: the whisker region of the primary somatosensory cortex (S1) and the ventral-posterior-medial (VPm) nucleus. These recordings were carried out while modulating the activity of L6 neurons locally using either bicuculline to enhance or muscimol to suppress their function. We observed that elevating the dynamics of L6 neurons led to a bidirectional adjustment of VPm neuron activity. Specifically, response magnitude increased for lower stimulus intensities and decreased for higher ones. Conversely, reducing the dynamics of L6 neurons resulted in a diminished response magnitude for lower stimulus intensities and augmentation for higher stimulus intensities. Modulating the dynamics of L6 neurons also resulted in a bidirectional modification of the degree to which VPm neurons could follow the stimulus and the degree of burstiness. Modulating the dynamics of L6 neurons also elicited a bidirectional alteration of the tactile discrimination of VPm neurons. Our findings reveal that cortical L6 neurons can modify pivotal aspects of thalamic sensory processing.

Materials and methods

Animals and surgery

Sprague–Dawley rats from both sexes (250–320 g) were anaesthetized with ketamine (100 mg/kg, I.P.; Ketaset; Fort Dodge Animal Health, Fort Dodge, IA, USA) and acepromazine maleate (1 mg/kg, I.P.; PromAce; Fort Dodge Animal Health). After tracheotomy, a short (1.5 cm) metal cannula (outer diameter (o.d.), 2 mm; inner diameter (i.d.), 1.5 mm) was inserted into the trachea. The rats were then placed in a standard stereotaxic device. Body temperature was kept at 37.0 ± 0.1°C using a heating blanket and a rectal thermometer (TC-1000; CWE, Ardmore, PA, USA). Anaesthesia was maintained using a mixture of halothane (0.5%–1.5%) and air employing artificial respiration at 100–115 bpm while monitoring end-tidal CO_2 levels and heart rate. Depth of anaesthesia was monitored based on the heart rate (250–450 bpm), eyelid reflex, pinch withdrawal and vibrissae movements. Halothane concentrations were set slightly above the level at which the first clear signs of vibrissae movements were observed while the eyelid reflex was still maintained. In some animals, we also used EEG recordings, obtained using two wires inserted under the skull at a distance of 10 mm anterocaudally. Based on these measurements, we determined the anaesthesia level in our recordings to be between stages III-2 and III-3 (Friedberg et al., 1999). After positioning the subjects in a stereotactic apparatus (TSE, Bad Homburg, Germany), we created an opening (1–2 mm in diameter) above the barrel cortex, centred at 2.5 mm posterior and 5.2 mm lateral to the bregma. Additionally, openings were made above the VPm thalamus, ranging from 2.56 to 4.3 mm posterior and 1.4 to 3.2 mm lateral to the bregma. VPm recordings were performed at depths ranging from 5.2 to 7.2 mm.

In some animals, we determined the correspondence between Microdrive depth and laminar identity. We induced electrolytic lesions using the recording electrodes by applying a direct current (10–30 μA) for 4 s at a depth corresponding to each recorded area. In some rats, brain tissues were also processed for cytochrome oxidase histochemistry. The animals were perfused transcardially with 2.5% glutaraldehyde and 0.5% paraformaldehyde, followed by 5% sucrose, all in 0.1 M phosphate-buffered saline (PBS). Brains from these rats were then transferred into a 30% sucrose postfixative solution and incubated overnight at 4°C. The following day, microtome cryosections (120 μm) were prepared and incubated in PBS containing 0.0015% cytochrome C (Sigma) and 0.05% diaminobenzidine 20–50 min at 37°C. The reaction was terminated by washing with PBS. CO-stained sections were mounted on gelatin-coated slides, air-dried and cover-slipped. Layers 2/3, 4, 5 and 6 were identified by recording depths of 150–550, 550–850, 900–1400 and

1400 μm and deeper, respectively. At the end of each experiment, animals were killed with an intraperitoneal injection of pentobarbital (150 mg/kg).

Recording technique

A multicontact silicone electrode (NeuroNexus, Ann Arbor, MI, USA) was inserted into the barrel cortex and the VPm. The electrode was lowered using a precision stereotactic micromanipulator (TSE-systems, Germany). During recording, signals were amplified (1000×), digitized (25 kHz), filtered (0.1–10,000 kHz) and stored for offline spike sorting and analysis using the ME-16 amplifier and MC-Rack software (MEA, Germany). Data were then separated into local field potentials (LFP; 1–150 Hz) and isolated single-unit activity (0.5–10 kHz). All neurons could be driven by the manual stimulation of one of the whiskers. Spike extraction and sorting were implemented using the MClust (by A.D. Redish; http://redishlab.neuroscience.umn.edu/MClust/MClust.html) MATLAB (Mathworks, Natick, MA, USA)-based spike-sorting software. The extracted and sorted spikes were stored at a 100 μs resolution, and peri-stimulus time histograms (PSTHs) were computed.

Intrinsic optical imaging

The principal whisker was identified using intrinsic optical imaging (Grinvald et al., 1986). Functional imaging was performed using a Qcam CCD camera (Q-imaging, Canada) equipped with a tandem lens system (DO-2595, F/0.95 and DO-5095, F/0.95, Navitar, NY, USA) and 610-nm LEDs (Telux VLWTG 9900, Vishay Electronic GmbH - Mouser electronics Mansfield, TX, USA) while stimulating a single whisker by a galvanometer (Model 6210H, Cambridge instruments, Watertown, MA, USA; 6-Hz deflections over 2-s duration) controlled via an isolated pulse stimulator (model 2100, A-M systems, Quebec, canada). The surface blood vessel pattern was imaged for reference. Image acquisition and analysis of the reflectance changes in the hemodynamic signal were performed using a frame grabber board (PCI-2110, National Instruments) and custom MATLAB software written in our laboratory. Images were acquired at a 10-Hz frame rate (200 frames per trial) with a 2 × 2 binning (∼300 × 300 pixels, 7.4 μm pixel size).

Whisker stimulation

Receptive fields were initially determined by manually deflecting individual vibrissae. Vibrissae that evoked detectable responses were individually attached to a computer-controlled galvanometer stimulator. We used two types of stimuli: The first was frozen Gaussian-filtered pseudorandom white noise (the size of the Gaussian window chosen resulted in a low-pass filter of about 250 Hz). Each stimulus was presented for 500 ms and repeated 25–50 times in the preferred orientation. The stimuli were played at 10 different variances per session (ranging between 70 and 692 μm, starting from the lowest variance the neuron responded to). A period of 2 s separated each stimulus. We ensured that the small variances would produce a low but consistent firing rate, and that the high variances would not cause saturation of the neuronal response. The second stimulus was a sine wave of varying amplitude and frequency. On each trial, the stimulus assumed 1 of 7 values (frequency: 20, 40, 60, 90, 140, 230 and 350 Hz; amplitude: 79.6, 192.3, 307.7, 153.8, 346.2 and 538.5 μm). The 42 frequency-amplitude combinations (termed *Af*, depicted in Fig. 6*A*) were presented 25–50 times per stimulus in a pseudorandom order. It has been shown that neurons explicitly encode the product of frequency and amplitude, which correlates with the mean vibration velocity (Arabzadeh et al., 2003). Based on this, we used the product of frequency and amplitude in our analysis of neuronal responses to sine wave stimuli.

Cortical drug application

We used a pulled glass capillary for cortical recording and drug application (WPI 504,949; o.d. = 1.14 mm; tip diameter approximately 70 μm) using a Sutter Instruments puller model P-97. We used the Axon Instruments AxoClamp 2B amplifier to record LFP signals and injected drugs through the same pipette using the Nanoliter 2010 (WPI). The solution within the pipette contained 1 mM bicuculine or 1 mM muscimol in a saline solution. The injected volumes were calibrated for each session to reduce LFP response by up to 85% of control. The injected volumes ranged between 800 and 2500 nl. The injected depth ranged from 1450 to 1700 μm.

As a tool for modifying cortical dynamics, we used muscimol and bicuculline. Although muscimol is primarily known as a $GABA_A$ receptor agonist (Johnston, 2013), some studies suggest that it may also have effects on $GABA_B$ receptors. $GABA_B$ receptors are metabotropic receptors that play a crucial role in modulating thalamocortical dynamics and synaptic plasticity. These receptors are expressed at thalamocortical terminals, where they modulate neurotransmitter release and neuronal excitability (Sanchez-Vives et al., 2021). Bicuculline is primarily known as a $GABA_A$ receptor antagonist (Johnston, 2013). However, several key studies have demonstrated that bicuculline can act on potassium channels, particularly small-conductance calcium-activated potassium (SK) channels (Debarbieux

et al., 1998). Despite these complex effects, we focus on the overall impact of these drugs on cortical dynamics.

Data analysis

Statistical analysis was performed using a one-way ANOVA to determine the significance of differences among the measured parameters. In cases where significant differences were detected in the F ratio test ($p < 0.05$), Tukey's multiple comparisons method was employed to identify specific pairs of measured parameters that exhibited significant differences from each other within a parameter group ($p < 0.01$). The mean values are presented with the corresponding SD. Error bars in all figures represent the SD unless otherwise stated.

Receiver operating characteristics analysis

We used signal detection theory (receiver operating characteristics (ROC) analysis (Green & Swets, 1974)) to compute the probability that an ideal observer could accurately determine the differences among the different textures based on neuronal activity. For each measured texture pair neuronal response, an ROC curve was constructed as a two-dimensional plot of hit probability (y-axis) and a false alarm (x-axis) probability. Green and Swets (1974) demonstrated that the area under the ROC curve (AUC) corresponds to the performance expected of an ideal observer in a two-alternative, forced-choice paradigm, such as the one used in the present analysis. The ROC curve was calculated for a single neuron's firing rate as a texture function. We then averaged all AUC values of all neurons and all texture pairs.

To transform raw data into a measure of discriminability, we analysed the distributions of neuronal firing rates across trials. The firing rate (Fr) in trial k is calculated as the spike count, Nsp_k, divided by T, the trial duration in milliseconds.

$$Fr = \frac{Nsp_k}{T}$$

The length T of the texture signal was set to 500 ms.

To assess the significance level of the AUC values we got from each neuron for all response comparisons, we shuffled the firing rates of all trials among the various responses. We then calculated the ROC curves and AUC values for the shuffled data. We then averaged all AUC values of all neurons and all texture pairs. This process was repeated 500 times. The significance level, set at mean + 2SD (95%), was AUC = 0.53.

Results

To investigate the impact of L6 feedback on sensory transmission in the VPm, we conducted *in vivo* electrophysiology recordings in lightly anaesthetized rats. During these recordings, we targeted the VPm and locally administered muscimol or bicuculline to the corresponding barrel in the cortex. We employed a range of whisker stimuli to analyse how L6 CT neurons affect the transformation of tactile stimuli into neuronal discharge characteristics in the VPm. Figure 1 illustrates the experimental set-up alongside examples demonstrating the effects of cortical drug applications on neuronal responses in the VPm.

Throughout this study, we use 'cortical dynamics' to refer to the complex, spatially organized activity patterns across frequency bands and cortical areas and their task-dependent modulations. This term also encompasses the relationship between LFPs and neural population activity, which varies across brain regions and behavioural states.

Figure 1*A* shows the schematic reciprocal anatomical connections between VPm and cortex and the experimental paradigm in which we record LFP, apply drugs through the same electrode in the principal barrel and record from the adjacent barrel. Concurrently, we recorded single-unit activity from the VPm during spontaneous and tactile responses. We initially removed the cranium above the barrel cortex to record and apply drugs in the corresponding barreloids and barrels and used intrinsic imaging to map all whisker responses (Grinvald et al., 1986) (Fig. 1*B*; see the Materials and Methods section). After establishing this mapping, we inserted an electrode into the VPm to isolate single-unit recordings. Through this process, we identified the primary whisker driving neuronal responses in the VPm. Subsequently, a glass pipette was inserted into the corresponding barrel in Layer 6 of the cortex. This allowed us to record LFP and administer drugs directly to the site. Additionally, in some experiments, another electrode was inserted into the cortex at a lateral distance of approximately 500 μm from the same depth to monitor activity in adjacent barrels.

Figure 1*D* and *G* displays Layer 6 LFP responses to 5 ms principal whisker stimulation under control conditions (black) and during local muscimol (C, red) or bicuculine application (D, blue). The adjacent barrel responses are depicted in green traces on the right panels. Across all sessions, our findings indicate that local muscimol application led to an average decrease of approximately 0.85 ± 0.15 compared to control responses ($n = 27$). The adjacent barrels displayed an average decrease of approximately 0.25 ± 0.15. On the contrary, bicuculine application resulted in an average enhancement of 0.6 ± 0.2 compared to control responses ($n = 24$). The adjacent

barrels displayed an average increase of approximately 0.15 ± 0.12. Additionally, we recorded spontaneous LFP activity under control conditions and during both drug applications. Quantifying the effects of the drugs via the total power in the power spectrum, we found that local muscimol application resulted in an average decrease in total LFP power compared to control responses (Fig. 1*E*). Conversely, bicuculine application led to an increase in total power compared to control responses (Fig. 1*F*).

Following cortical drug application, we investigated their impact on spontaneous and sensory-evoked activity in the VPm. We used two types of stimuli: sine waves at various frequencies and amplitudes and filtered white noise at different amplitudes, as described in the Materials

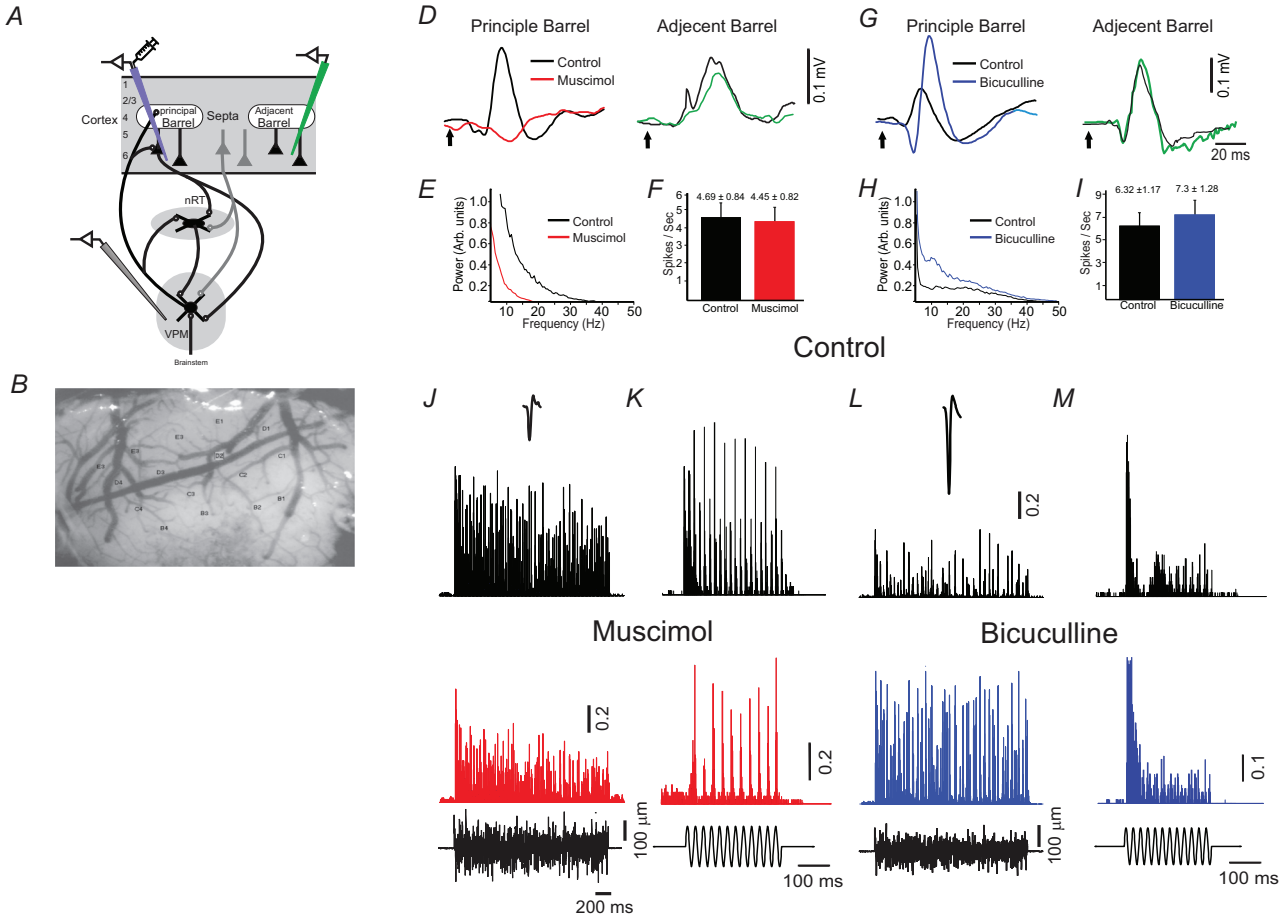

Figure 1. The influence of Layer 6 drug application on ventral-posterior-medial (VPm) responses
A, schematic reciprocal anatomical connections between VPm and cortex and the experimental paradigm in which we record local field potentials (LFP), apply drugs through the same electrode in the principal barrel and record from the adjacent barrel. Concurrently, we recorded single-unit activity from the VPm during spontaneous and tactile responses. *B*, mapping of the corresponding whiskers' barrels using intrinsic imaging. *C* and *D*, layer 6 LFP responses to 5 ms principal whisker stimulation under control conditions (black) and during local muscimol application (*C*, red) or bicuculine application (*D*, blue). The adjacent barrel responses are depicted in green traces on the right panels. *E* and *F*, quantifying the effects of the drugs via the total power in the power spectrum of spontaneous LFP activity. Local muscimol application resulted in a decrease in total LFP power compared to control responses. *E*, conversely, the bicuculine application increased total power compared to control responses (*F*). *G* and *H*, the impact of cortical drug application on spontaneous firing rates in the VPm. Muscimol application (*G*, red) or bicuculine application (*H*, blue) showed no significant influence on the firing rates of VPm neurons. *I–L*, the impact of cortical drug application on sensory-evoked responses of two VPm neurons. Peri-stimulus time histograms (PSTHs) of a VPm neuron responding to white noise stimuli (*I, K*) and sine wave stimuli (*J, L*) are shown. The upper panels represent control conditions, whereas the middle panels display neuronal responses during muscimol application (*I, J*, red) or bicuculine application (*K, L*, blue). The lower panels display the whisker stimuli. Muscimol cortical application reduced firing rates in this neuron, whereas bicuculine application led to increased firing rates. The waveforms shown in *I* and *K* represent spike waveforms obtained from spike-sorted VPm recordings. The vertical scale bar for PSTH shows the spike probability/millisecond bin. [Colour figure can be viewed at wileyonlinelibrary.com]

and Methods section. The cortical application of these drugs did not affect spontaneous activity in the VPm for either of the drugs, as illustrated in Fig. 1*G* ($n = 27$) and 1*H* ($n = 24$). Examples of two VPm neurons responding to the two types of stimuli during the control condition are depicted in the upper panels of Fig. 1*J*–*M*. At the same time, their responses during the cortical application of both drugs are shown in the lower panels. These examples demonstrate that the cortical application of L6 muscimol led to decreased response magnitude in the VPm, whereas bicuculine application increased response magnitude.

Previous research has shown that cortical neurons respond to the product of stimulus amplitude and frequency (*Af*), which represents velocity, rather than to frequency or amplitude independently (Arabzadeh et al., 2003). Therefore, to assess how well VPm neurons can distinguish between different stimuli, we converted the sine wave frequency and amplitude combinations into their corresponding velocity (*Af*) values. Figure 6*A* provides a greyscale visualization of these various stimulus combinations regarding their velocity. We used SD to quantify differences in stimulus intensity for white noise stimuli.

Bidirectional impact of bicuculine and muscimol

We employed filtered, frozen white noise stimuli varying in different amplitudes to examine the influence of bicuculine and muscimol L6 application on VPm sensory-evoked responses. Examples of two VPm neurons responding to the stimuli during the control condition are depicted in the upper panels of Fig. 2*A* and *B*. Their responses during the cortical application of both drugs are shown in the lower panels for the neurons in Fig. 2*A* and *B*. We plot the relationship between stimulus amplitude, measured by the SD, and neuronal firing rates in Fig. 2*C* and *D*. We demonstrate that these relationships can be fitted with linear regression. More importantly, we demonstrate two opposing effects depending on stimulus SD. At lower stimulus SD, cortical bicuculine application increased VPm neuronal response magnitude, whereas muscimol application decreased response magnitude (see left panels of Fig. 2*C* and *D*). In contrast, cortical bicuculine application decreased VPm neuronal response magnitude at higher stimulus SD, whereas muscimol application increased response magnitude (see right panels of Fig. 2*C* and *D*).

For each neuron, we computed the stimulus amplitude at the point of response reversal, where the response magnitude transitions significantly from increasing to decreasing or vice versa compared to the control. This reversal point was typically around SD $= 0.8 \pm 0.2 \times 10^3$ μm for white noise stimuli. Subsequently, for each neuron, we partitioned the relationship between stimulus and response into enhanced and decreased response segments (Fig. 2*C* and *D*). To quantify these changes, we calculated the ratio between the firing rates at each stimulus SD in the control condition and during drug application. If all the points show a significant increase or decrease in firing rates, they were included in the respective groups (enhanced responses, reduced responses, no change).

We found that during bicuculine application at low stimulus intensities, most neurons ($n = 23$; 68%) show an increase in firing rates (Fig. 2*E*, left bars), whereas larger stimulus intensities resulted in a decrease in firing rates (78%). We plotted the ratios in the two groups (enhanced and decreased) to quantify these changes, as shown in Fig. 2*F* ($p = 1.253 \times 10^{-7}$, based on a binomial exact test). During muscimol application, we observed that most neurons ($n = 26$; 63%) exhibited decreased firing rates at low stimulus intensities (Fig. 2*G*, left bars). In contrast, higher stimulus intensities led to an increase in firing rates in 66% of neurons. To quantify these effects, we calculated the ratios of neurons with increased *versus* decreased firing rates, as illustrated in Fig. 2*F*, with statistical significance determined by a binomial exact test ($p = 1.051 \times 10^{-6}$). These results suggest that the dynamics of L6 neurons impact the responses of VPm neurons in a stimulus-dependent manner.

We applied the same analysis to sine wave stimuli with varying *Af* (Fig. 1*C*). Examples of two VPm neurons' responses during control conditions are shown in the upper panels of Fig. 3*A* and *B*, whereas their responses during cortical drug application are displayed in the lower panels. By plotting the relationship between stimulus frequency (at a constant amplitude of 76.9 μm) and neuronal firing rates in Fig. 3*C* and *D*, we found that these relationships can be fitted with a sigmoidal function (see the Materials and Methods section). Similar to white noise stimuli, we observed two opposing effects depending on stimulus *Af*: Cortical bicuculine application increased VPm neuronal response magnitude at lower amplitudes, whereas muscimol application decreased it (Fig. 3*C* and *D*). Conversely, cortical bicuculine application at higher *Af* decreased VPm neuronal response magnitude, whereas muscimol application increased it (not shown). As before, for each neuron, we calculated the stimulus *Af* at the point of response reversal, where the response magnitude transitions from increasing to decreasing or vice versa compared to the control. We then segmented the relationship between stimulus and response into enhanced and decreasing. To quantify the effects of the drugs, we fitted each neuron's responses with a sigmoidal function and extracted three parameters: the slope, the maximal point and a shift in the slope. Subsequently, we calculated the ratios between control conditions and drug application in the two groups (increasing and decreasing). During bicuculine application at low stimulus intensities, all neurons ($n = 27$) exhibited a decrease in the slope (less

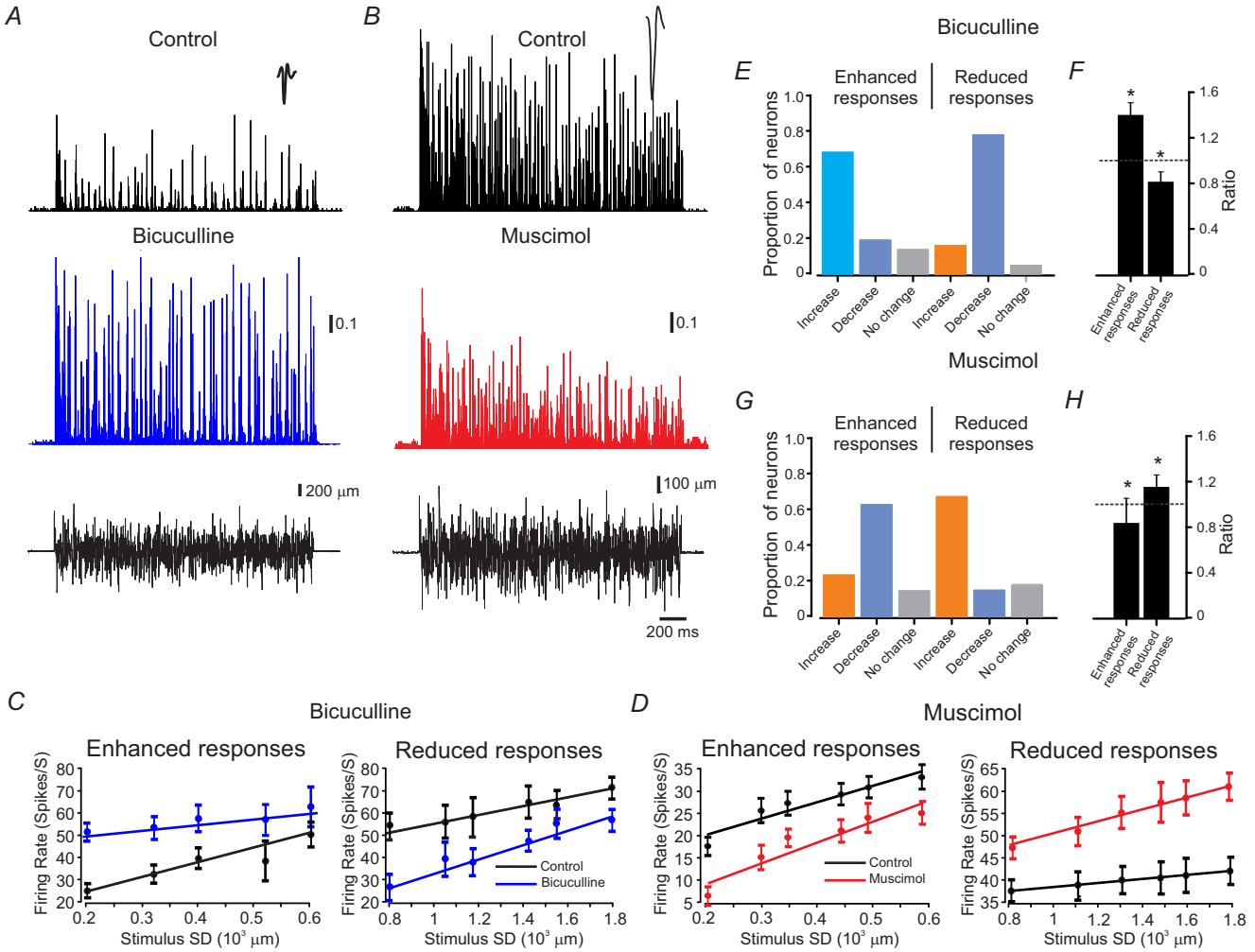

Figure 2. Assessing the impact of cortical drug application on ventral-posterior-medial (VPm) neuronal responses to a white noise stimulus
A and *B*, the impact of cortical drug application on sensory-evoked responses of two VPm neurons. Peri-stimulus time histograms (PSTHs) of a VPm neuron responding to white noise stimuli are shown. The upper panels represent control conditions, whereas the middle panels display neuronal responses during muscimol (red) or bicuculine application (blue). The lower panels display the whisker stimuli. *C*, examining the neuron in *A* across a wide range of stimulus SD, we observed that during control conditions (black), firing rates increased as a function of SD. However, during the bicuculine application, firing rates increased for lower stimulus intensities (left panel) and decreased for higher (right panel). *D*, examining the neuron in *B* across a wide range of stimulus SD, we observed that during control conditions (black), firing rates increased as a function of SD. However, during the muscimol application, firing rates decreased for lower stimulus intensities (left panel) and increased for higher stimulus intensities (right panel). *E*, quantifying the proportions of neurons that increased, decreased or showed no change in firing rates during bicuculine application in response to low and high stimulus magnitudes (SD). Enhanced responses – 0.68 increase, 0.19 decrease and 0.13 no change. Reduced responses – 0.17 increase, 0.78 decrease and 0.05 no change. *F*, the relative changes in firing rates during the bicuculine application that resulted in enhanced responses (1.38) and during reduced responses (0.81). *G*, quantifying the proportions of neurons that increased, decreased or showed no change in firing rates during the muscimol application in response to low and high stimulus magnitudes (SD). Enhanced responses – 0.24 increase, 0.62 decrease and 0.14 no change. Reduced responses – 0.67 increase, 0.15 decrease and 0.18 no change. *H*, the relative changes in firing rates during bicuculine application that resulted in enhanced responses (0.82) and during reduced responses (1.15). The waveforms shown in *A* and *B* represent spike waveforms obtained from spike-sorted VPm recordings. The vertical scale bar for PSTH shows the spike probability/millisecond bin. [Colour figure can be viewed at wileyonlinelibrary.com]

steep), a leftward shift in the fit and an increase in the maximal point. However, at higher stimulus intensities, only the maximal point was reduced (Fig. 3*E*, slope: 0.81 ± 0.08, $p = 0.67 \times 10^{-5}$; maximum: 1.18 ± 0.06, $p = 0.86 \times 10^{-4}$, shift low *Af*: 0.79 ± 0.19, $p = 0.77 \times 10^{-5}$, maximum high *Af*: 0.71 ± 0.15, $p = 1.145 \times 10^{-3}$, based on a binomial exact test). During muscimol application at low stimulus intensities, all neurons ($n = 23$) exhibited a significant increase in the slope (Fig. 3*F*, slope: 1.54 ± 0.07, $p = 0.56 \times 10^{-7}$). Together, these findings demonstrate the stimulus magnitude-dependent impact of cortical L6 on VPm tactile response transformation.

VPm adaptation is modulated by L6 dynamics

Behaviourally relevant inputs for rats involve sequences of whisker stimuli occurring during rhythmic whisker movements (Deschenes et al., 2003) against objects

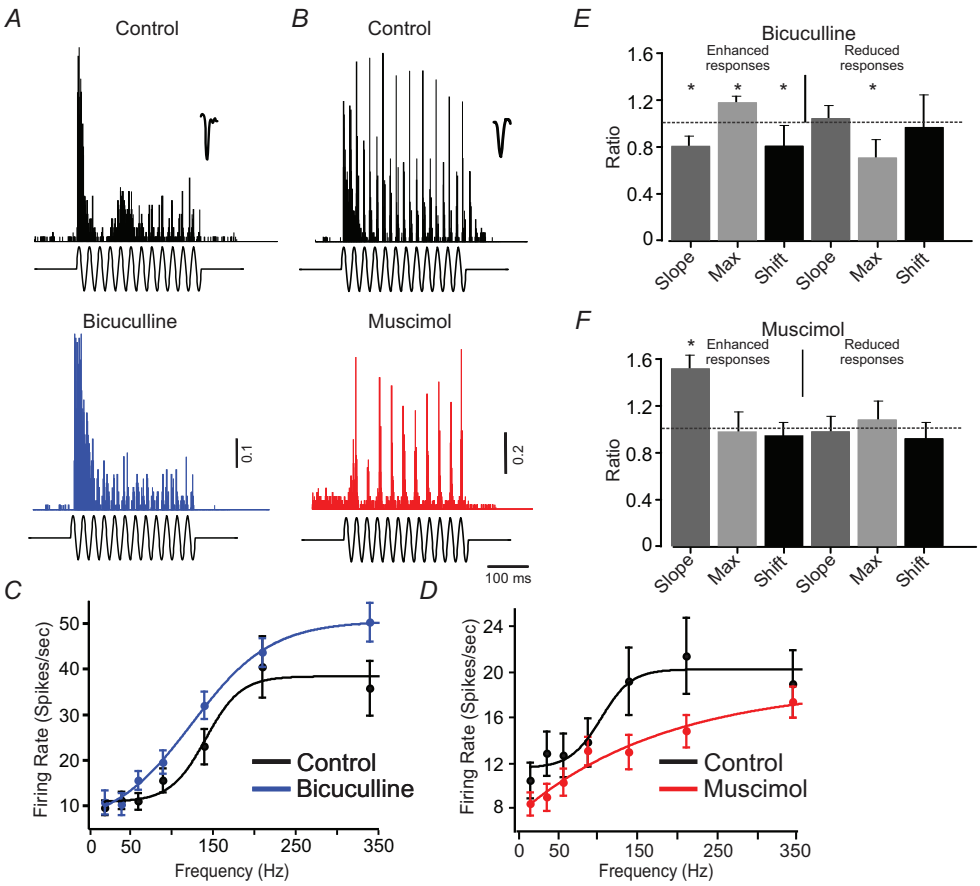

Figure 3. Assessing the impact of cortical drug application on ventral-posterior-medial (VPm) neuronal responses to sine wave stimulus
A and *B*, the impact of cortical drug application on sensory-evoked responses of two VPm neurons. Peri-stimulus time histograms (PSTHs) of a VPm neuron responding to sine wave stimuli are shown. The upper panels represent control conditions, whereas the middle panels display neuronal responses during the muscimol (red) or bicuculine application (blue). The lower panels display the whisker stimuli. *C*, examining the neuron in *A* across a wide range of stimulus frequencies at an amplitude of 76.9 μm, we observed that during control conditions (black), firing rates increased as a function of frequency. However, during the bicuculine application, firing rates increased. *D*, examining the neuron in *B* across a wide range of frequencies, we observed that during control conditions (black), firing rates increased as a function of frequencies. However, during the application of muscimol, there was a notable alteration in the relationship between stimulus frequencies and neuronal firing rates. These alterations manifested in significant changes in the maximal firing rates, the slope of the fitted curve and the overall shift in the response curve. *E*, quantifying the relative changes in characteristics of the sigmoidal fit to the data: the slope, the maximal firing rates and a shift in the slope. When bicuculline was applied, there was an observed increase in maximal firing rates at low *Af*, accompanied by a reduction in slope and a leftward shift of the curve. Only a reduction in the maximal firing rates was observed at higher *Af*. *F*, when muscimol was applied, an increase in slope was observed at lower *Af*. The waveforms shown in *A* and *B* represent spike waveforms obtained from spike-sorted VPm recordings. The vertical scale bar for PSTH shows the spike probability/millisecond bin. [Colour figure can be viewed at wileyonlinelibrary.com]

and exploration and when the whiskers are swept across surfaces (Wolfe et al., 2008). As in other sensory thalamocortical systems, VPm neurons exhibit characteristic rapid adaptation to sensory inputs (Castro-Alamancos, 2002b), (Ahissar et al., 2000; Castro-Alamancos, 2002b). Due to this rapid adaptation, spiking in response to initial stimuli is highly probable, but later stimuli in a sequence are transmitted less reliably. We employed sine wave stimuli at various frequencies, as well as at lower and larger amplitudes. To quantify the tracking of neuronal responses, we used the fast Fourier transform (FFT) on the filtered spike trains (see the Materials and Methods section). We then analysed the temporal modulations of neuronal responses to the stimuli. The modulation index (MI) was employed to detect and assess the strength of these modulations. The MI is defined as the ratio of the magnitude of the response (area in the FFT) at the fundamental temporal frequency of the stimulus (F1 component) to the magnitude of the averaged net response, or, assuming very low background ('spontaneous') activity, over the magnitude of the averaged response (F0; see Fig. 4*C*).

In Fig. 4*A* an example response of a VPm neuron is depicted. The PSTH indicates that the neuron could track the stimulus. Following the application of muscimol, the neuron exhibited a slight reduction in firing rates (22.3 ± 5.2 to 18.2 ± 3.8). However more notably, the responses of this neuron ceased to track the stimulus. To characterize the entire population of recorded neurons ($n = 18$), we plotted the MI before and during bicuculine and muscimol applications in response to low and high stimulus amplitudes. Following the bicuculine application VPm neurons increased their MI by 1.9 ± 0.01 for low stimulus intensities and 1.2 ± 0.1 for enhanced responses. However this increase was not statistically significant (two-way ANOVA; $p = 0.49 \times 10^{-5}$). Figure 4*E* shows the impact of muscimol application on the MI of VPm neurons ($n = 20$). VPm neurons decreased their MI by 0.63 ± 0.05 for enhanced responses and 0.96 ± 0.05 for reduced responses, although this decrease was not statistically significant (two-way ANOVA; $p < 1.2 \times 10^{-7}$). These results suggest that L6 cortical neurons modulate the ability of VPm neurons to track tactile stimuli.

VPm burst propensity is regulated by L6 dynamics

The duality of thalamic response mode is a crucial property of thalamic information processing, influencing how sensory input reaches the cortex. The burst mode involves relayed sensory inputs as short, rapid clusters of spikes, whereas the tonic mode translates the same inputs into a single spike. To investigate the impact of L6 input on sensory responses in the VPm, we initially assessed spike responses to filtered white noise stimulus while manipulating the L6 to VPm pathway. We initially calculated the inter-spike-interval histogram (ISIH) for all responses and all conditions. An example of ISIH of the response of a neuron to low amplitude stimulus condition during control condition and bicuculine application is shown in Fig. 5*A* and *B*. Prior studies have demonstrated that bursts are reflected in a second peak in the ISIH (Nowak et al., 2003). To quantify response burstiness, we computed the total number of spikes between 10 and 20 ms of the ISIH and divided this number by the total number of spikes between 1 and 10 ms. This ratio measured the relative number of spikes within bursts *versus* single spikes. Cortical L6 bicuculine application ($n = 17$) led to a significant increase in the ratio from 0.11 ± 0.2 to 0.19 ± 0.25 (two-way ANOVA; $p = 1.75 \times 10^{-6}$), whereas muscimol application ($n = 20$) resulted in a significant decrease in the ratio from 0.24 ± 0.1 to 0.13 ± 0.04 (two-way ANOVA; $p = 2.05 \times 10^{-5}$). These results suggest that L6 cortical neurons regulate the firing mode of VPm neurons.

VPm stimulus discrimination is regulated by L6 dynamics

We employed ideal observer analysis to evaluate the influence of L6 on VPm neuronal discrimination. We compared the firing rates across all trials for all stimuli. To evaluate the discriminatory ability of each neuron, we employed the area under the ROC curve (AUC) measure. The AUC value quantitatively measures the neuron's ability to discriminate between the stimuli, with higher values indicating better discrimination. We calculated the AUC for each neuron across all possible combinations of *Af* values. Fig. 6*B* illustrates an example of a neuron responding to two stimuli with different SDs. Figure 6*C* shows the corresponding ROC curve and the associated AUC for a neuron in Fig. 6*B*. The inset displays the distribution of firing rates for the two stimuli. Fig. 6*D* shows the average AUC values across all stimuli. This figure uses a colour-coded pixel-based matrix representation, where each pixel corresponds to the average AUC value for a specific stimuli combination in this specific neuron.

We analysed every possible combination of SD and *Af* in reaction to white noise and sine wave stimuli. This analysis was performed under both control conditions and cortical drug application. Figure 7 illustrates the mean AUC values for all neurons across each stimuli SD and *Af* comparison. For instance, Fig. 7*A* displays various combinations of sine wave stimuli converted into *Af* values on the *x*-axis. We plot the difference between all *Af* values to compute the discrimination among these stimuli. Likewise, for white noise stimuli in Fig. 7*B*, we illustrate the variance in

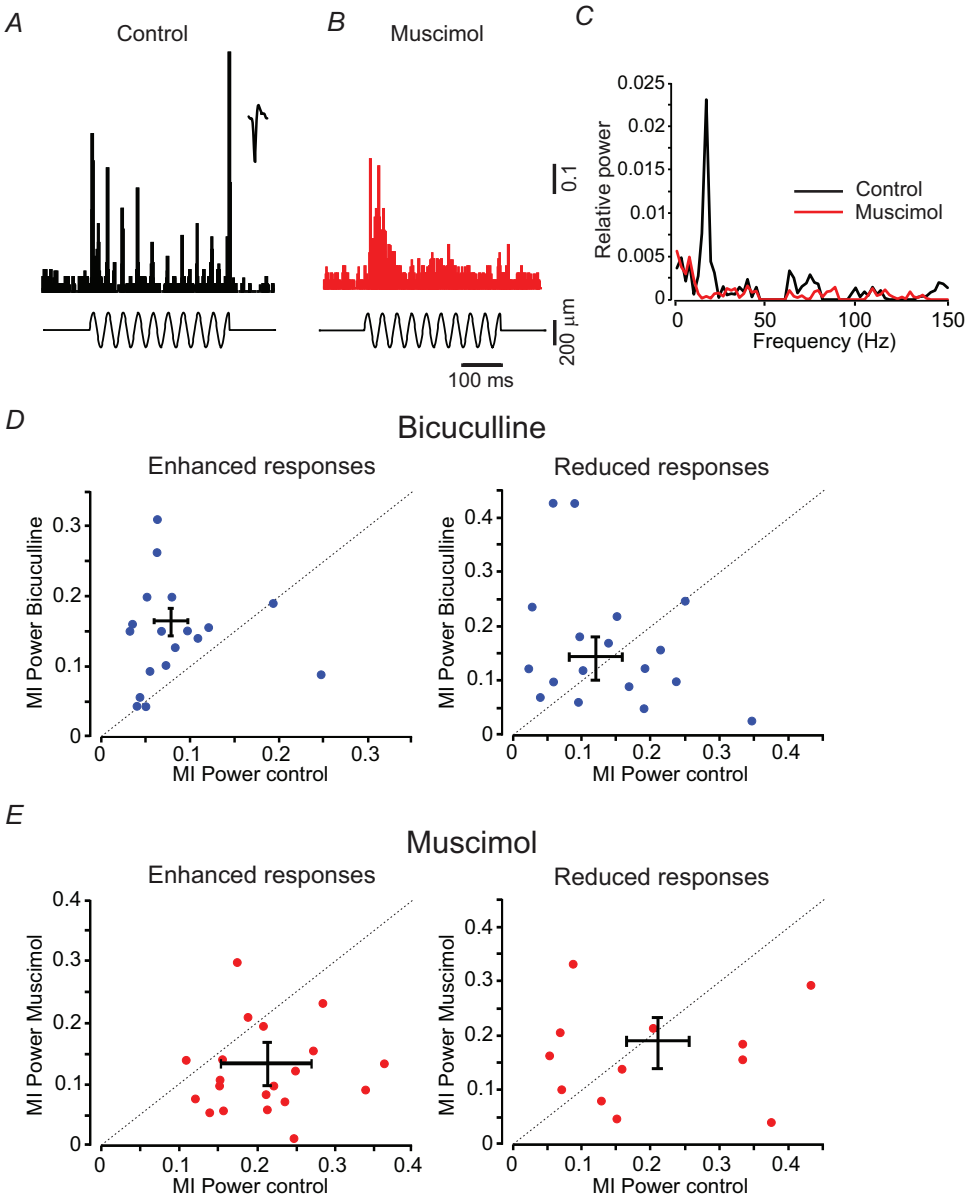

Figure 4. Assessing the impact of cortical drug application on ventral-posterior-medial (VPm) neuronal responses adaptation

A and *B*, the impact of cortical drug application on sensory-evoked responses. Peri-stimulus time histograms (PSTHs) of a VPm neuron responding to sine wave stimuli are shown. The panels in *A* represent control conditions, whereas the panels in *B* display neuronal responses during the muscimol application (red). The lower panels display the whisker stimuli. *C*, the power spectrum analysis of the neuronal response in *A* and *B* revealed that the locking with the stimulus was abolished. *D*, before and during the L6 bicuculine application, the modulation index (MI) was measured in response to stimuli with lower and higher *Af*. During application, VPm neurons showed increased MI of 1.9 ± 0.01 for lower *Af* and 1.2 ± 0.1 for higher *Af* (left panel), with the latter not reaching statistical significance (right panel). The diagonal line indicates the equality value. *E*, the impact of L6 muscimol application on the MI of VPm neurons was assessed. Muscimol application decreased MI by 0.63 ± 0.05 for lower *Af* and 0.96 ± 0.05 for higher *Af*, though the reduction for higher *Af* did not reach statistical significance. The waveform shown in *A* represents spike waveforms obtained from spike-sorted VPm recordings. The diagonal line indicates the equality value. The vertical scale bar for PSTH shows the spike probability/millisecond bin. [Colour figure can be viewed at wileyonlinelibrary.com]

Table 1. The average AUC ratio comparing reduced and enhanced responses under control conditions (black lines in Fig. 7) and during Bicuculline (blue lines) and Muscimol application (red lines).

Stimulus	Control	Bicuculine	Muscimol
Sine wave	1.79 ± 0.23	1.18 ± 0.03 (n = 22)	2.04 ± 0.12 (n = 26)
White noise	1.1 ± 0.1	2.3 ± 0.14 (n = 21)	0.35 ± 0.11 (n = 23)

stimuli magnitude by depicting the disparity in SD. Our findings suggest that increasing the difference between stimuli improves discrimination, as evidenced by larger AUC values (Fig. 7, black lines). No discrimination was detected for slight differences in stimuli, as indicated by AUC values falling below the significance line (dashed line at AUC = 0.54). At more significant differences in stimuli, we observed AUC values as high as 0.9 in response to white noise and sine wave stimuli. We then explored the ability of VPm neurons to distinguish between various stimuli at both lower and higher magnitudes, resulting in increased or decreased responses during drug application, as indicated by the left and right columns, respectively.

In all experiments, we observed that VPm neurons exhibited superior discrimination between stimuli at higher stimulus intensities than lower ones. To quantify this, we calculated the average AUC values for each plot (represented by black lines). We derived the ratios between the averages of higher *Af* stimuli (right column) and lower-magnitude stimuli (left column). These values were compared under control conditions and during bicuculine (indicated by blue lines) and muscimol applications (indicated by red lines), as shown in Table 1. Under control conditions, VPm neurons demonstrated superior discrimination ability for higher *Af* sine wave stimuli compared to lower *Af* ones (Fig. 7*A*). Bicuculine drastically reduced this ratio, whereas muscimol increased it. In contrast, no difference in discrimination ability was observed between higher- and lower-SD white noise stimuli under control conditions. However, bicuculine significantly increased this ratio, whereas muscimol decreased it. These results suggest that lowering cortical dynamics increases discrimination in response to high *Af* sine wave stimuli but decreases it for low *Af*, whereas the opposite effects occur for white noise stimuli.

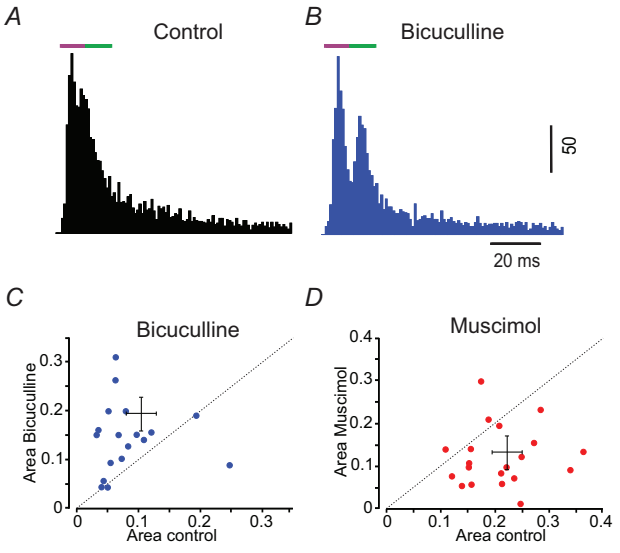

Figure 5. Assessing the impact of cortical drug application on ventral-posterior-medial (VPm) neuronal responses burst propensity
A and *B*, an example of inter-spike-interval histograms (ISIHs) is the response of a neuron to low amplitude stimulus conditions during control condition (*A*) and bicuculine application (*B*). To quantify response burstiness, we calculated the ratio of spikes occurring between 10 and 20 ms (horizontal purple bar) to those between 1 and 10 ms (horizontal green bar) in the ISIH. *C*, applying bicuculine resulted in a significant increase in the ratio from 0.11 ± 0.2 to 0.19 ± 0.25. *D*, muscimol application resulted in a significant decrease in the ratio from 0.24 ± 0.1 to 0.13 ± 0.04. [Colour figure can be viewed at wileyonlinelibrary.com]

Following this, we compared these control conditions with those where bicuculine and muscimol were applied to the cortex. We observed that bicuculine application resulted in a moderate increase in stimulus discrimination for sine wave stimuli during lower stimulus intensities (Fig. 7*A* left panel). This increase was measured by calculating the ratios of each point (above the significance level) in the plot. These calculations revealed an increase of 1.26. In contrast, at higher stimulus intensities, bicuculine application resulted in a moderate decrease in stimulus discrimination (Fig. 7*A*, right panel; ratio = 0.86). Similarly, the impact of cortical muscimol application resulted in a moderate increase in stimulus discrimination during lower stimulus intensities (Fig. 7*C*, left panel; ratio = 1.21). At higher stimulus intensities, muscimol application resulted in a moderate increase in stimulus discrimination (Fig. 7*C*, right panel; ratio = 1.08).

In contrast to the moderate changes observed in discrimination in response to sine wave stimuli, cortical drug application resulted in substantial alterations in discrimination in response to white noise stimulation. We found that bicuculine application significantly increased stimulus discrimination for white noise stimuli during lower stimulus intensities (Fig. 7*B*, left panel; ratio = 1.92; for enhanced responses). In contrast, at higher

stimulus intensities, the bicuculine application did not change stimulus discrimination (Fig. 7*B*, right panel; ratio = 0.99; for reduced responses). Similarly, the impact of cortical muscimol application resulted in a significant decrease in stimulus discrimination during lower stimulus intensities (Fig. 7*D*, left panel; ratio = 0.49; for enhanced responses). At higher stimulus intensities, muscimol application also led to a moderate increase in stimulus discrimination (Fig. 7*D*, right panel; ratio = 1.1; for reduced responses). These findings suggest that cortical dynamics plays a significant role in influencing the discrimination capabilities of VPm

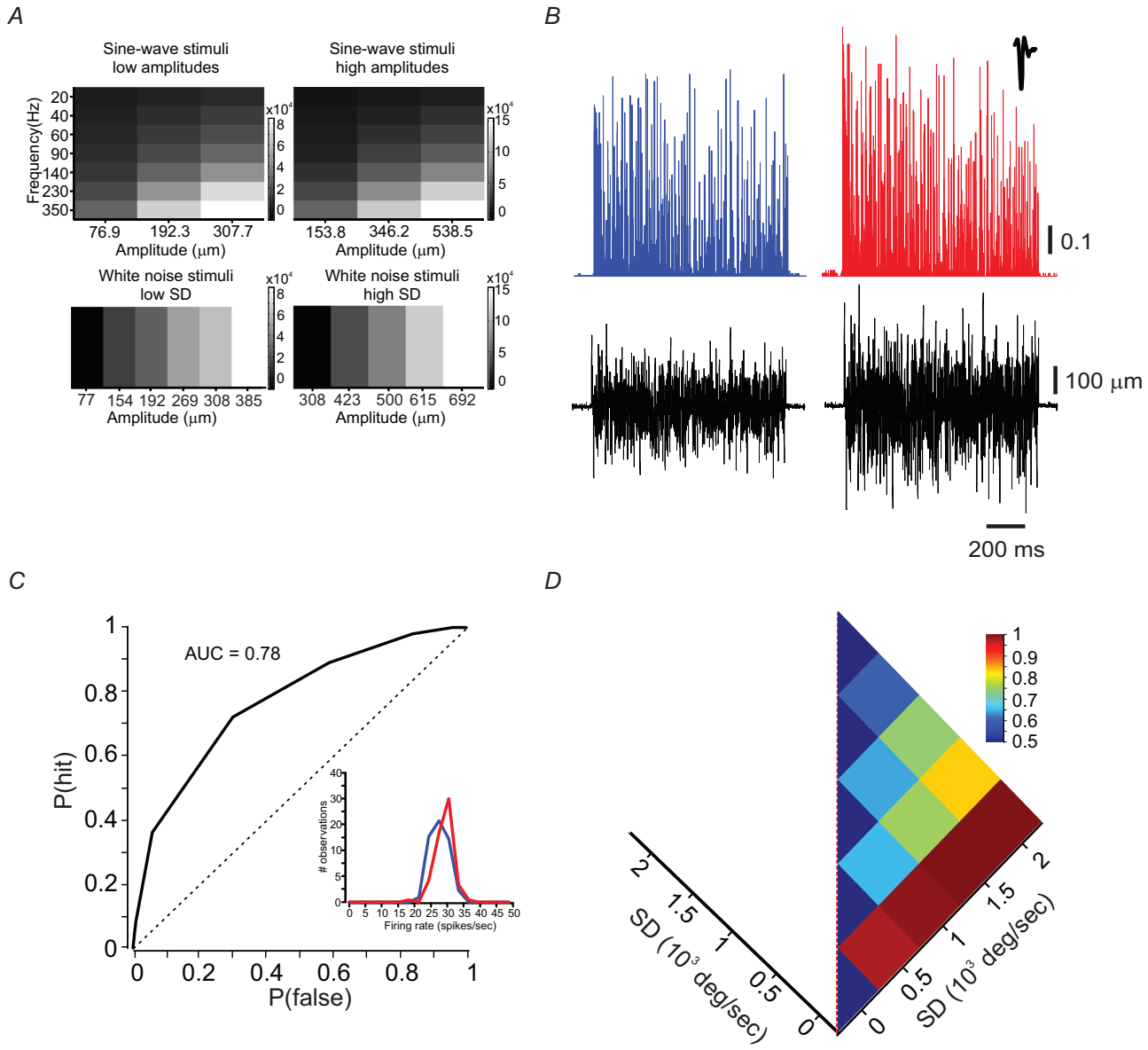

Figure 6. Assessing neuronal discrimination using receiver operating characteristics (ROC) analysis
A, visual representation of the stimuli used in the experiment. It showcases the sine wave frequency and amplitude stimuli transformed into *Af* values, as described in the Materials and Methods section. The figure also includes illustrations of the white noise stimuli, with variations in magnitude indicated by the stimulus's SD measure. *B*, peri-stimulus time histograms (PSTHs) of a ventral-posterior-medial (VPm) neuron responding to white noise stimuli at two stimulus magnitudes are shown. The lower panels show stimulus. The vertical scale bar for PSTH shows the spike probability/millisecond bin. *C*, the area under the curve (AUC), based on the ROC analysis, was calculated for the two stimuli in (*B*), yielding an AUC value of 0.78. The inset depicts the firing rate distribution for the two stimuli. *D*, a colour-coded matrix illustrates the AUC values for the five stimuli. Each square within the matrix corresponds to an average AUC value. The waveform shown in *B* represents spike waveforms obtained from spike-sorted VPm recordings. [Colour figure can be viewed at wileyonlinelibrary.com]

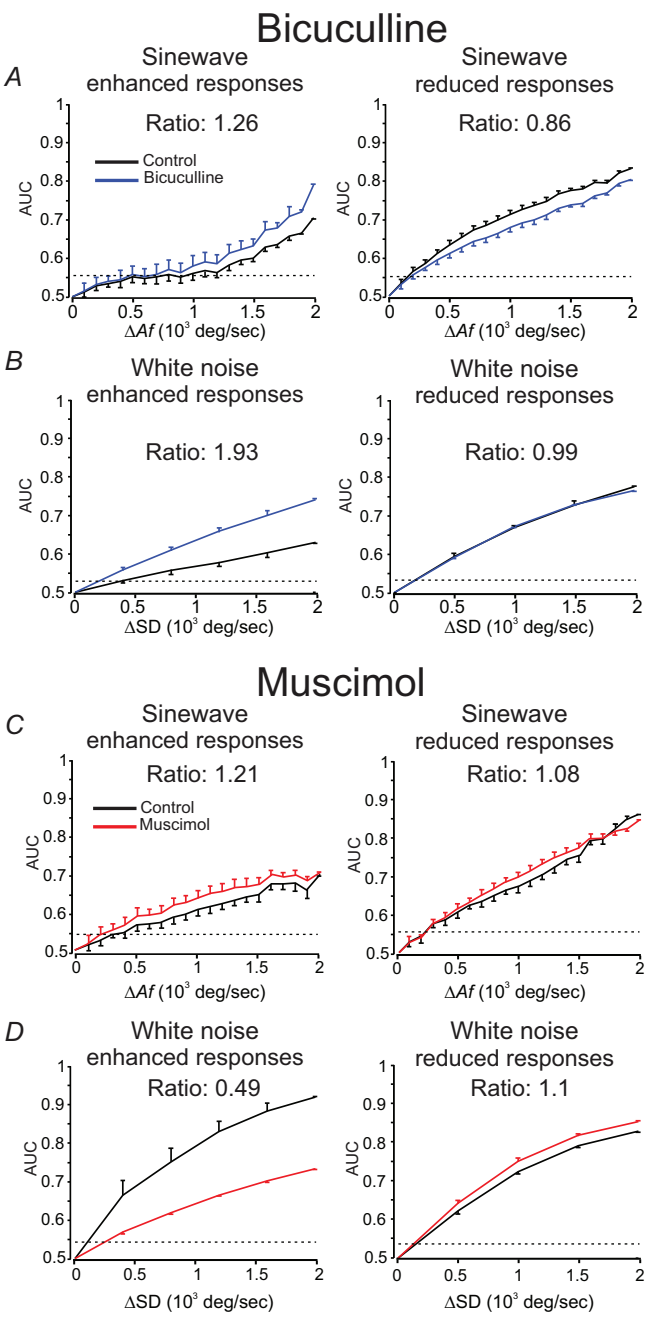

Figure 7. Assessing the impact of cortical drug application on ventral-posterior-medial (VPm) stimuli discrimination
A, the effect of Bicuculline on tactile discrimination was analysed for Δ*Af* for sine wave stimuli. Each point on the *x*-axis represents a different Δ*Af* value, whereas the *y*-axis displays all neurons' average ± SD of the area under the curve (AUC). As Δ*Af* increases, so does the AUC. The dashed horizontal line represents the significance level of shuffled trials (see the Materials and Methods section). The ratio was computed for all points located above the significance level. The left panel illustrates these relationships for low *Af* sine wave, whereas the right panel displays the results for high *Af*. *B*, the effect of bicuculine on tactile discrimination was analysed for ΔSD for white noise stimuli. Each point on the *x*-axis represents a different ΔSD value, whereas the *y*-axis displays all neurons' average ± SD of the AUC. As ΔSD increases, so does the AUC. The dashed horizontal line represents the significance level of shuffled trials (see the Materials and Methods section). The ratio was computed for all points located above the significance level. The left panel illustrates these relationships for low white noise amplitudes, whereas the right panel displays the results for high amplitudes. *C*, the effect of Muscimol on tactile discrimination was analysed for Δ*Af* for sine wave stimuli similar to panel *A*. *D*, the effect of Muscimol on tactile discrimination was analysed for Δ*Af* for sine wave stimuli similar to panel *A*. [Colour figure can be viewed at wileyonlinelibrary.com]

neurons across various stimuli. Specifically, we identified a direct connection between cortical activity and sensory information processing in the VPm region.

Discussion

In this study we aimed to investigate the transmission of tactile signals through the whisker somatosensory thalamus. These processes are dynamic, marked by bidirectional communication between the cortex and thalamus. It underscores the significant impact of cortical activity on thalamic function and, by extension, its processing of tactile whisker input. We used numerous tactile stimuli to investigate how different patterns of whisker deflection modulate neural activity in the somatosensory thalamus. The main objective was to understand the thalamic processing and representation of tactile information and to examine how altering cortical dynamics in L6 influences these processes.

Cortical dynamics significantly influenced VPm neuron response magnitude in a stimulus-intensity-dependent manner. Increasing L6 dynamics (via bicuculine) increased firing rates at low intensities but decreased them at higher intensities (Fig. 2*E,F*). In contrast, decreasing L6 dynamics (via muscimol) had opposite effects (Fig. 2*G,H*). Analysis of sine wave stimuli revealed a sigmoidal relationship between stimulus frequency and firing rates (Fig. 3). Increased L6 dynamics decreased and shifted the response slope leftward, increased maximum response at low intensities, but decreased it at higher intensities (Fig. 3*E,F*).

We described an L6 corticothalamic circuit (Fig. 1*A*) that dynamically modulates tactile-evoked VPm activity, switching between suppression and enhancement based on activity levels (Fig. 3). This illustrates the cortex's role as an activity-dependent gatekeeper of sensory input. Increased L6 dynamics enhanced tactile detection and discrimination at lower stimulus intensities but reduced these at higher intensities. Decreased L6 dynamics had opposite effects. Analysis of VPm responses to sine wave stimuli showed that L6 dynamics affect neuronal response magnitude in a stimulus amplitude-dependent manner. At low intensities, increased L6 dynamics decreased

the slope, shifted the sigmoidal function leftward and raised its maximal point, whereas decreased dynamics increased the slope. These findings highlight the complex differential modulation of VPm responses by cortical L6 based on stimulus amplitude.

These findings suggest that cortical dynamics significantly influence the discrimination capabilities of VPm neurons across various stimuli. Changes in discrimination following the application of cortical drugs, such as bicuculine and muscimol, highlight a direct link between cortical activity and sensory information processing in the VPm. The substantial increase in discrimination with bicuculine at lower stimulus intensities suggests enhanced sensory processing under heightened cortical dynamics. Conversely, the moderate decrease in discrimination at higher intensities with bicuculine may indicate a disruption in sensory processing due to excessive cortical activity. Similarly, muscimol application, resulting in a significant increase in discrimination at lower intensities and a modest increase at higher intensities, further emphasizes the complex relationship between cortical activity and VPm neuron discrimination.

Sensory signals undergo significant transformations in the thalamus, with sensory adaptation being a critical process. Thalamic sensory adaptation, marked by decreased firing rates during prolonged stimulation (Castro-Alamancos, 2002a; Diamond et al., 1992; Simons & Carvell, 1989, b), reduces the transmission efficacy of subsequent stimuli to the cortex, potentially enhancing the encoding of small changes (Barlow, 1961; Fairhall et al., 2001; Wark et al., 2007). Adapting to tactile stimuli can enhance or impair sensory processing in the whisker system, depending on the behavioural context (Lampl & Katz, 2017; Mohar et al., 2015; Musall et al., 2014; Ollerenshaw et al., 2014). Our findings show that increasing L6 dynamics reduces adaptation to whisker deflections in the VPm (Fig. 4*D*, left panel), whereas decreasing L6 dynamics enhances it (Fig. 4*E*, left panel), particularly at lower stimulus amplitudes. At higher stimulus amplitudes, cortical dynamics has a minor impact on thalamic adaptation (Fig. 4*D* and *E*, right panels). These results suggest that L6 control of VPm adaptation operates as a continuous and dynamic modulator, adjusting thalamic adaptation based on cortical dynamics in real time. This control mechanism fine-tunes sensory processing to meet the immediate demands of the sensory environment and behavioural context. Robust L6 activity reduces adaptation, benefiting high-frequency tactile inputs such as texture or vibration discrimination. Although higher input frequencies decrease individual neuronal response probability, population coding compensates, improving signal processing accuracy (Abbott & Dayan, 1999; Farkhooi et al., 2013; Liu et al., 2017), but see Sharma and Azouz (2022). Conversely, diminished L6 activity increases thalamic adaptation, which would be detrimental to texture or vibration discrimination.

An additional aspect of tactile thalamic processing is the duality of thalamic response modes, bursting and tonic modes, which are crucial in how tactile inputs reach the cortex. Both modes occur during anaesthesia/sleep and wakefulness/behaviour, with a shift towards tonic mode during alertness (Fanselow et al., 2001; Guido & Weyand, 1995; Halassa et al., 2011; Ramcharan et al., 2000; Slézia et al., 2011). Thalamic bursts may signal novel stimuli to the cortex, whereas tonic mode allows for linear encoding of fine stimulus details, such as during object examination (Crick, 1984; Sherman, 2001). Understanding burst/tonic responses is challenging due to the unknown involvement of the cortex in rapid firing mode changes observed in awake and anaesthetized animals (Bezdudnaya et al., 2006; Guido & Weyand, 1995; Mease et al., 2014).

Our findings challenge the classical view of thalamic function. Previous studies proposed that VPm neurons switch between a burst mode, which suppresses sensory information relay, and a tonic mode for transmission. However, our data reveal a broader spectrum of firing patterns in VPm neurons, not limited to distinct bursts. This continuum of activity suggests a more nuanced role for VPm neurons.

We also observed the coexistence of burst and tonic responses to sensory stimuli, aligning with other research in awake and anaesthetized animals. Increased L6 dynamics boost thalamic burst propensity, improving the processing of high-frequency tactile inputs such as texture or vibration discrimination. Conversely, reduced L6 activity diminishes thalamic burst propensity, negatively impacting texture or vibration discrimination. Our study provides a more sophisticated understanding of VPm neuron function, moving beyond the simplistic on/off switch model of burst activity and sensory relay.

The main difference between our findings and those from optogenetic studies is the nature of neural activation. Optogenetic techniques typically employ patterned, periodic and synchronized stimulation, offering precise temporal control over specific neuronal populations. This approach allows for investigating neural circuits with high temporal resolution and cell-type specificity. In contrast, our methodology involves a more generalized modulation of neural dynamics, resulting in elevated or reduced activity across the targeted neuronal population. Although less temporally precise, this approach provides insights into altered neural activity's broader, sustained effects on sensory processing and behaviour.

Our method of inducing generalized changes in dynamics allows us to examine the overall impact of altered cortical activity on thalamic function, potentially mimicking more naturalistic fluctuations in brain states. On the contrary optogenetic studies excel at dissecting

the specific roles of neural circuits with millisecond-scale precision. By comparing results from these diverse approaches, we can better understand neural modulation, encompassing precise, rhythm-driven effects and broader, state-dependent changes in neural processing. This multifaceted view is crucial for elucidating the complex dynamics of sensory information processing in the thalamocortical system.

Plausible neuronal mechanisms

Studies in thalamocortical brain slices have shown that L6 neurons can affect thalamic dynamics by combining monosynaptic excitation and disynaptic inhibition in the VPm thalamus (Crandall et al., 2015; McCormick & von Krosigk, 1992; Mease et al., 2014). These studies showed that the modulation mode of L6 neurons can dynamically mediate either synaptic suppression or enhancement based on the frequency and timing of their activation (Crandall et al., 2015). Thus corticothalamic influence is dynamic, shifting between enhancement and suppression based on activity levels. Recent *in vivo* studies have demonstrated that L6 CT neurons can enhance or suppress the gain of thalamic sensory responses (Born et al., 2021; Denman & Contreras, 2015; Mease et al., 2014; Olsen et al., 2012; Pauzin & Krieger, 2018; Spacek et al., 2022; Temereanca & Simons, 2004). Our findings show corticothalamic neurons can bidirectionally adjust thalamic excitability and sensory throughput. These changes in thalamic transformation rely on various forms of short-term synaptic plasticity across cortico-thalamic circuits. Thus diminished cortical activity evokes prolonged inhibitory signals in the thalamus, effectively suppressing sensory input to the cortex. Conversely higher firing rates in L6 neurons enhance sustained sensory responses by reducing adaptation in thalamic neurons (Mease et al., 2014; Sillito et al., 1994). This ultimately strengthens the thalamic drive to the cortex, potentially including a feedback loop involving CT cells (Alonso et al., 1996; Averbeck et al., 2006; Cruikshank et al., 2007; Yang et al., 2014). However research suggests low CT firing can also trigger bursts in relay cells under specific resting membrane states (Hirsch et al., 1983; Jahnsen & Llinás, 1984a, b, c; Steriade et al., 1993). In summary L6 modulates sensory signal processing within the thalamocortical system. It influences the depolarization, membrane potential noise and conductance of thalamic neurons (Wolfart et al., 2005), fine-tuning sensory information from the thalamus to the cortex.

Functional implications

We have shown that L6 CT feedback plays a crucial role in modulating sensory processing, serving as a key mechanism for gain control in thalamocortical circuits. Controlling thalamic adaptation and sensory relay modes allows the cortex to influence its sensory input, modulating thalamic excitability and the strength and precision of sensory signals (Mease et al., 2014). This adaptive control enables the cortex to fine-tune sensory processing in response to environmental demands.

In vision circuits L6 CT feedback provides robust gain control by adjusting the strength of sensory input relative to background activity (Born et al., 2021; Spacek et al., 2022). This mechanism amplifies salient sensory features while suppressing irrelevant inputs, supporting efficient sensory discrimination. CT feedback can also switch thalamic processing between feature detection and discrimination modes (Guo et al., 2017), enabling flexible sensory processing based on task demands. The influence of CT feedback is particularly robust for naturalistic stimuli, such as movie responses in mice's dorsal lateral geniculate nucleus (Spacek et al., 2022), and these effects interact with the behavioural state (Kimberly et al., 2023).

During wakefulness, CT feedback actively modulates the somatosensory thalamocortical circuit, with its effects depending on the brain state (Dimwamwa et al., 2024). During alert states, CT feedback enhances gain to prioritize behaviourally relevant stimuli, whereas in low-arousal states, it reduces gain, leading to a relative suppression of sensory input. Additionally, L6 CT ensembles can selectively regulate sensory salient stimuli, behavioural impact and cortical representation (Voigts et al., 2020). This function highlights salient or unexpected stimuli, enhancing their prominence in sensory representations, which may play a key role in attentional selection and prediction error signalling. Finally, CT feedback circuits also play a role in motor control (Martinetti et al., 2024), suggesting a potential link to sensorimotor integration.

Overall, L6 CT feedback operates as a dynamic and sophisticated gain control system, modulating thalamic sensory processing to adjust sensory circuit sensitivity based on context, task demands and brain state. By regulating thalamic relay modes, enhancing salient features and suppressing irrelevant inputs, it fine-tunes the flow of sensory information to meet environmental and behavioural demands across various sensory modalities, ensuring efficient, flexible and context-dependent cortical processing.

References

Abbott, L. F., & Dayan, P. (1999). The effect of correlated variability on the accuracy of a population code. *Neural Computation*, **11**(1), 91–101.

Adams, P., Guillery, R. W., Sherman, S. M., Sillito, A. M., Sherman, S. M., & Guillery, R. W. (2002). The role of the thalamus in the flow of information to the cortex. *Philosophical Transactions of the Royal Society of London Series B: Biological Sciences*, **357**(1428), 1695–1708.

Ahissar, E., Sosnik, R., & Haidarliu, S. (2000). Transformation from temporal to rate coding in a somatosensory thalamocortical pathway. *Nature*, **406**(6793), 302–306.

Alonso, J. M., Usrey, W. M., & Reid, R. C. (1996). Precisely correlated firing in cells of the lateral geniculate nucleus. *Nature*, **383**(6603), 815–819.

Arabzadeh, E., Petersen, R. S., & Diamond, M. E. (2003). Encoding of whisker vibration by rat barrel cortex neurons: Implications for texture discrimination. *Journal of Neuroscience*, **23**(27), 9146–9154.

Averbeck, B. B., Latham, P. E., & Pouget, A. (2006). Neural correlations, population coding and computation. *Nature Reviews Neuroscience*, **7**(5), 358–366.

Barlow, H. (1961). Possible principles underlying the transformations of sensory messages. *Sensory Communication*, **1**.

Bezdudnaya, T., Cano, M., Bereshpolova, Y., Stoelzel, C. R., Alonso, J. M., & Swadlow, H. A. (2006). Thalamic burst mode and inattention in the awake LGNd. *Neuron*, **49**,3, 421–432.

Binzegger, T., Douglas, R. J., & Martin, K. A. (2007). Stereotypical bouton clustering of individual neurons in cat primary visual cortex. *Journal of Neuroscience*, **27**(45), 12242–12254.

Born, G., Schneider-Soupiadis, F. A., Erisken, S., Vaiceliunaite, A., Lao, C. L., Mobarhan, M. H., Spacek, M. A., Einevoll, G. T., & Busse, L. (2021). Corticothalamic feedback sculpts visual spatial integration in mouse thalamus. *Nature Neuroscience*, **24**(12), 1711–1720.

Bortone Dante, S., Olsen Shawn, R., & Scanziani, M. (2014). Translaminar inhibitory cells recruited by layer 6 corticothalamic neurons suppress visual cortex. *Neuron*, **82**(2), 474–485.

Bourassa, J., & Deschêˆnes, M. (1995). Corticothalamic projections from the primary visual cortex in rats: A single fiber study using biocytin as an anterograde tracer. *Neuroscience*, **66**(2), 253–263.

Briggs, F., Kiley Caitlin, W., Callaway Edward, M., & Usrey, W. M. (2016). Morphological substrates for parallel streams of corticogeniculate feedback originating in both V1 and V2 of the macaque monkey. *Neuron*, **90**(2), 388–399.

Castro-Alamancos, M. A. (2002*a*). Different temporal processing of sensory inputs in the rat thalamus during quiescent and information processing states in vivo. *The Journal of Physiology*, **539**(2), 567–578.

Castro-Alamancos, M. A. (2002*b*). Properties of primary sensory (lemniscal) synapses in the ventrobasal thalamus and the relay of high-frequency sensory inputs. *Journal of Neurophysiology*, **87**(2), 946–953.

Crandall Shane, R., Cruikshank Scott, J., & Connors Barry, W. (2015). A corticothalamic switch: Controlling the thalamus with dynamic synapses. *Neuron*, **86**(3), 768–782.

Crick, F. (1984). Function of the thalamic reticular complex: The searchlight hypothesis. *Proceedings of the National Academy of Sciences of the USA*, **81**(14), 4586–4590.

Cruikshank, S. J., Lewis, T. J., & Connors, B. W. (2007). Synaptic basis for intense thalamocortical activation of feedforward inhibitory cells in neocortex. *Nature Neuroscience*, **10**(4), 462–468.

Debarbieux, F., Brunton, J., & Charpak, S. (1998). Effect of bicuculline on thalamic activity: A direct blockade of I AHP in reticularis neurons. *Journal of Neurophysiology*, **79**(6), 2911–2918.

Denman, D. J., & Contreras, D. (2015). Complex effects on in vivo visual responses by specific projections from mouse cortical layer 6 to dorsal lateral geniculate nucleus. *Journal of Neuroscience*, **35**(25), 9265–9280.

Deschenes, M., Timofeeva, E., & Lavallee, P. (2003). The relay of high-frequency sensory signals in the Whisker-to-barreloid pathway. *Journal of Neuroscience*, **23**(17), 6778–6787.

Diamond, M. E., Armstrong-James, M., & Ebner, F. F. (1992). Somatic sensory responses in the rostral sector of the posterior group (POm) and in the ventral posterior medial nucleus (VPM) of the rat thalamus. *Journal of Comparative Neurology*, **318**(4), 462–476.

Dimwamwa, E. D., Pala, A., Chundru, V., Wright, N. C., & Stanley, G. B. (2024). Dynamic corticothalamic modulation of the somatosensory thalamocortical circuit during wakefulness. *Nature Communications*, **15**(1), 3529.

Fairhall, A. L., Lewen, G. D., Bialek, W., & de Ruyter Van Steveninck, R. R. (2001). Efficiency and ambiguity in an adaptive neural code. *Nature*, **412**(6849), 787–792.

Fanselow, E. E., Sameshima, K., Baccala, L. A., & Nicolelis, M. A. (2001). Thalamic bursting in rats during different awake behavioral states. *Proceedings National Academy of Science USA*, **98**(26), 15330–15335.

Farkhooi, F., Froese, A., Muller, E., Menzel, R., & Nawrot, M. P. (2013). Cellular adaptation facilitates sparse and reliable coding in sensory pathways. *PLoS Computational Biology*, **9**(10), e1003251.

Friedberg, M. H., Lee, S. M., & Ebner, F. F. (1999). Modulation of receptive field properties of thalamic somatosensory neurons by the depth of anaesthesia. *Journal of Neurophysiology*, **81**(5), 2243–2252.

Green, D. M., & Swets, J. A. (1974). *Signal detection theory and psychophysics*. R. E. Krieger Pub. Co., Huntington, N.Y.,.

Grinvald, A., Lieke, E., Frostig, R. D., Gilbert, C. D., & Wiesel, T. N. (1986). Functional architecture of cortex revealed by optical imaging of intrinsic signals. *Nature*, **324**(6095), 361–364.

Groh, A., de Kock, C. P., Wimmer, V. C., Sakmann, B., & Kuner, T. (2008). Driver or coincidence detector: Modal switch of a corticothalamic giant synapse controlled by spontaneous activity and short-term depression. *Journal of Neuroscience*, **28**(39), 9652–9663.

Guido, W., & Weyand, T. (1995). Burst responses in thalamic relay cells of the awake behaving cat. *Journal of Neurophysiology*, **74**(4), 1782–1786.

Guo, W., Clause, A. R., Barth-Maron, A., & Polley, D. B. (2017). A corticothalamic circuit for dynamic switching between feature detection and discrimination. *Neuron*, **95**(1), 180–194.e5.

Halassa, M. M., Siegle, J. H., Ritt, J. T., Ting, J. T., Feng, G., & Moore, C. I. (2011). Selective optical drive of thalamic reticular nucleus generates thalamic bursts and cortical spindles. *Nature Neuroscience*, **14**(9), 1118–1120.

Hirsch, J. C., Fourment, A., & Marc, M. E. (1983). Sleep-related variations of membrane potential in the lateral geniculate body relay neurons of the cat. *Brain Research*, **259**(2), 308–312.

Jahnsen, H., & Llinás, R. (1984*a*). Electrophysiological properties of guinea-pig thalamic neurones: An in vitro study. *The Journal of Physiology*, **349**(1), 205–226.

Jahnsen, H., & Llinás, R. (1984*b*). Ionic basis for the electro-responsiveness and oscillatory properties of guinea-pig thalamic neurones in vitro. *The Journal of Physiology*, **349**(1), 227–247.

Jahnsen, H., & Llinás, R. (1984*c*). Voltage-dependent burst-to-tonic switching of thalamic cell activity: An in vitro study. *Archives Italiennes De Biologie*, **122**(1), 73–82.

Johnston, G. A. (2013). Advantages of an antagonist: Bicuculline and other GABA antagonists. *British Journal of Pharmacology*, **169**(2), 328–336.

Kim, J., Matney, C. J., Blankenship, A., Hestrin, S., & Brown, S. P. (2014). Layer 6 corticothalamic neurons activate a cortical output layer, layer 5a. *Journal of Neuroscience*, **34**(29), 9656–9664.

Kimberly, R., Arbora, R., & Massimo, S. (2023). Brain state-dependent modulation of thalamic visual processing by cortico-thalamic feedback. *The Journal of Neuroscience*, **43**(9), 1540.

Lampl, I., & Katz, Y. (2017). Neuronal adaptation in the somatosensory system of rodents. *Neuroscience*, **343**, 66–76.

Lefort, S., Tomm, C., Floyd Sarria, J. C., & Petersen, C. C. (2009). The excitatory neuronal network of the C2 barrel column in mouse primary somatosensory cortex. *Neuron*, **61**(2), 301–316.

Liu, C., Foffani, G., Scaglione, A., Aguilar, J., & Moxon, K. A. (2017). Adaptation of thalamic neurons provides information about the spatiotemporal context of stimulus history. *Journal of Neuroscience*, **37**(41), 10012–10021.

Liu, X.-B., Honda, C. N., & Jones, E. G. (1995). Distribution of four types of synapse on physiologically identified relay neurons in the ventral posterior thalamic nucleus of the cat. *Journal of Comparative Neurology*, **352**(1), 69–91.

Llano, D. A., & Sherman, S. M. (2008). Evidence for nonreciprocal organization of the mouse auditory thalamocortical-corticothalamic projection systems. *Journal of Comparative Neurology*, **507**(2), 1209–1227.

Martinetti, L. E., Autio, D. M., & Crandall, S. R. (2024). Motor control of distinct layer 6 corticothalamic feedback circuits. *eNeuro*, **11**(7). https://doi.org/10.1101/2024.04.22.590613

McCormick, D. A., & von Krosigk, M. (1992). Corticothalamic activation modulates thalamic firing through glutamate" metabotropic" receptors. *Proceedings of the National Academy of Sciences*, **89**(7), 2774–2778.

Mease, R. A., Krieger, P., & Groh, A. (2014). Cortical control of adaptation and sensory relay mode in the thalamus. *Proceedings of the National Academy of Sciences*, **111**(18), 6798–6803.

Mohar, B., Ganmor, E., & Lampl, I. (2015). Faithful representation of tactile intensity under different contexts emerges from the distinct adaptive properties of the first somatosensory relay stations. *Journal of Neuroscience*, **35**(18), 6997–7002.

Musall, S., Von Der Behrens, W., Mayrhofer, J. M., Weber, B., Helmchen, F., & Haiss, F. (2014). Tactile frequency discrimination is enhanced by circumventing neocortical adaptation. *Nature Neuroscience*, **17**(11), 1567–1573.

Nowak, L. G., Azouz, R., Sanchez-Vives, M. V., Gray, C. M., & McCormick, D. A. (2003). Electrophysiological classes of cat primary visual cortical neurons in vivo as revealed by quantitative analyses. *Journal of Neurophysiology*, **89**(3), 1541–1566.

Ollerenshaw, D. R., Zheng, H. J. V., Millard, D. C., Wang, Q., & Stanley, G. B. (2014). The adaptive trade-off between detection and discrimination in cortical representations and behavior. *Neuron*, **81**(5), 1152–1164.

Olsen, S. R., Bortone, D. S., Adesnik, H., & Scanziani, M. (2012). Gain control by layer six in cortical circuits of vision. *Nature*, **483**(7387), 47–52.

Pauzin, F. P., & Krieger, P. (2018). A corticothalamic circuit for refining tactile encoding. *Cell Reports*, **23**(5), 1314–1325.

Ramcharan, E. J., Gnadt, J. W., & Sherman, S. M. (2000). Burst and tonic firing in thalamic cells of unanesthetized, behaving monkeys. *Visual Neuroscience*, **17**(1), 55–62.

Sanchez-Vives, M. V., Barbero-Castillo, A., Perez-Zabalza, M., & Reig, R. (2021). GABA(B) receptors: Modulation of thalamocortical dynamics and synaptic plasticity. *Neuroscience*, **456**, 131–142.

Sharma, H., & Azouz, R. (2022). Coexisting neuronal coding strategies in the barrel cortex. *Cerebral Cortex*, **32**(22), 4986–5004.

Sherman, S. M. (2001). Tonic and burst firing: Dual modes of thalamocortical relay. *Trends in Neuroscience (Tins)*, **24**(2), 122–126.

Sherman, S. M., & Koch, C. (1986). The control of retinogeniculate transmission in the mammalian lateral geniculate nucleus. *Experimental Brain Research*, **63**(1), 1–20.

Sillito, A. M., Jones, H. E., Gerstein, G. L., & West, D. C. (1994). Feature-linked synchronization of thalamic relay cell firing induced by feedback from the visual cortex. *Nature*, **369**(6480), 479–482.

Simons, D. J., & Carvell, G. E. (1989). Thalamocortical response transformation in the rat vibrissa/barrel system. *Journal of Neurophysiology*, **61**(2), 311–330.

Slézia, A., Hangya, B., Ulbert, I., & Acsády, L. (2011). Phase advancement and nucleus-specific timing of thalamocortical activity during slow cortical oscillation. *Journal of Neuroscience*, **31**(2), 607–617.

Spacek, M. A., Crombie, D., Bauer, Y., Born, G., Liu, X., Katzner, S., & Busse, L. (2022). Robust effects of cortico-thalamic feedback and behavioral state on movie responses in mouse dLGN. *eLife*, **11**, e70469.

Steriade, M., McCormick, D. A., & Sejnowski, T. J. (1993). Thalamocortical oscillations in the sleeping and aroused brain. *Science*, **262**(5134), 679–685.

Temereanca, S., & Simons, D. J. (2004). Functional topography of corticothalamic feedback enhances thalamic spatial response tuning in the somatosensory whisker/barrel system. *Neuron*, **41**(4), 639–651.

Thomson, A. M. (2010). Neocortical layer 6, a review. *Frontiers in Neuroanatomy*, **4**, 13.

van Horn, S. C., Erişir, A., & Sherman, S. M. (2000). Relative distribution of synapses in the A-laminae of the lateral geniculate nucleus of the cat. *Journal of Comparative Neurology*, **416**(4), 509–520.
Voigts, J., Deister, C. A., & Moore, C. I. (2020). Layer 6 ensembles can selectively regulate the behavioral impact and layer-specific representation of sensory deviants. *eLife*, **9**, e48957.
Wark, B., Lundstrom, B. N., & Fairhall, A. (2007). Sensory adaptation. *Current Opinion in Neurobiology*, **17**(4), 423–429.
Winer, J. A., Diehl, J. J., & Larue, D. T. (2001). Projections of auditory cortex to the medial geniculate body of the cat. *Journal of Comparative Neurology*, **430**(1), 27–55.
Wolfart, J., Debay, D., Le Masson, G., Destexhe, A., & Bal, T. (2005). Synaptic background activity controls spike transfer from thalamus to cortex. *Nature Neuroscience*, **8**(12), 1760–1767.
Wolfe, J., Hill, D. N., Pahlavan, S., Drew, P. J., Kleinfeld, D., & Feldman, D. E. (2008). Texture coding in the rat whisker system: Slip-stick versus differential resonance. *PLoS Biology*, **6**(8), e215.
Yang, Q., Chen, C.-C., Ramos, R. L., Katz, E., Keller, A., & Brumberg, J. C. (2014). Intrinsic properties of and thalamocortical inputs onto identified corticothalamic-VPM neurons. *Somatosensory & Motor Research*, **31**(2), 78–93.
Zhang, Z.-W., & Deschênes, M. (1997). Intracortical axonal projections of lamina VI cells of the primary somatosensory cortex in the rat: A single-cell labeling study. *The Journal of Neuroscience*, **17**(16), 6365–6379.

Additional information

Data availability statement

All data presented in the figures of this article are available for access at the following link: https://drive.google.com/drive/folders/1At_VEj0UKrf_IH1sQUiha2p7n1Q8qbpx?usp = sharing. This repository includes raw and processed datasets used in our analyses, ensuring transparency and reproducibility.

Competing interests

All authors affirm that they have no competing interests or conflicts of interest related to the publication of this article.

Author contributions

A.E. did the acquisition and analysis of the data. R.A. contributed to the conceptualization and design of the study, interpreted the data and authored the manuscript. All authors approved the final version of the manuscript and agree to be accountable for all aspects of the work in ensuring that questions related to the accuracy or integrity of any part of the work are appropriately investigated and resolved. All persons designated as authors qualify for authorship, and all those who qualify for authorship are listed.

Funding

Israel Science Foundation (ISF). Grant number : 482/25

Acknowledgements

This work was supported by a grant from the Israel Science Foundation to R.A.

Keywords

cortex, perceptual constancy, sensory processing, somatosensory system, textures, whiskers

Supporting information

Additional supporting information can be found online in the Supporting Information section at the end of the HTML view of the article. Supporting information files available:

Peer Review History